Large edge-magnetism in oxidized few-layer black phosphorus nanomeshes

Y. Nakanishi[1], A. Ishii[2], C. Ohata[1], D. Soriano[3], R. Iwaki[1], K. Nomura[1], M. Hasegawa[2], T. Nakamura[5], S. Katsumoto[5], S. Roche[3,4], J. Haruyama[1]

[1] *Faculty of Science and Engineering and* [2]*Chemistry and Biological Science, Aoyama Gakuin University, 5-10-1 Fuchinobe, Sagamihara, Kanagawa 252-5258, Japan*

[3] *ICN2-Institut Catala de Nanociencia i Nanotecnologia, Campus UAB, 08193 Bellaterra (Barcelona), Spain*

[4] *Institució Catalana de Recerca i Estudis Avançats (ICREA), Barcelona, 08070, Spain*

[5] *Institute for Solid State Physics, The University of Tokyo, 5-1-5 Kashiwanoha, Kashiwa, Chiba277-8581, Japan*

The formation and control of a room-temperature magnetic order in two-dimensional (2D) materials is a challenging quest for the advent of innovative magnetic- and spintronic-based technologies. To date, edge magnetism in 2D materials has been experimentally observed in hydrogen (H)-terminated graphene nanoribbons and graphene nanomeshes (GNM), but the measured magnetization remain far too small to allow envisioning practical applications. Herein, we report experimental evidences of room-temperature large edge ferromagnetism in oxygen (O)-terminated few-layer black phosphorus nanomeshes (BPNMs). The magnetization values per unit area are ~100 times larger than those reported for H-terminated GNMs, and magnetism is absent for H-terminated BPNMs. Magnetization measurements and First-principles simulations suggest that the origin of such magnetic order could stem from a ferromagnetic coupling between edge P with O atoms, resulting in a strong spin localization at edge valence band, and from an uniform oxidation of pore edges over large area without the formation of a bulk oxide. Our findings pave the way for realizing high-efficiency 2D flexible magnetic and spintronic devices without the use of rare magnetic elements.

Achieving room-temperature magnetic order in 2D materials is one of the main challenge to create novel spin functionalities[1,2]. Such quest embraces a vast field of research, from harvesting magnetic proximity effects using graphene in close contact with strong spin-orbit coupling materials and magnetic oxides[3,4] to defect engineering for the creation of robust magnetic moments with the possible emergence of long-range ordering[5]. Long range magnetic ordering at room temperature could be used to monitor spin propagation in a nearby graphene layer, opening unprecedented perspectives for spin manipulation and spin-based information processing technologies. Recently atomic-scale engineering of graphene edges with zigzag-type atomic structure has been shown to give rise to a robust magnetic order[6]. Indeed, flat energy bands hand high electronic density of states (the so-called edge states) form in zigzag graphene nanoribbons, leading to robust spin polarization (i.e., flat-band ferromagnetism (FM)) [7-18]. Flat-band FM has been also demonstrated through in H-terminated zigzag-edged GNMs consisting of a honeycomb-like array of hexagonal nano-pores (similar to Fig. 1E), fabricated using a non-lithographic method, resulting in low-disordered and low-contaminated pore edges[11-18]. Because a GNM roughly correspond to a large ensemble of zigzag-edged graphene nanoribbons (GNRs), which are 1D strip lines of graphene, small magnetic signals arising from the pore edge spins can be easily detected. Nevertheless, the observed magnetization values so far have been as small as ~10^{-6} emu [12,13], except for some specific case using an electron beam resist treatment [14].

On the other hand, mono- or few-layer BP have recently been predicted as 2D semiconductors with substantial energy band gaps[19,20]. BP has a puckered honeycomb lattice, easily oxidized under air atmosphere exposure, with an in-plane anisotropic atomic structure (i.e., zigzag within monolayer and buckling armchair formed over two layers; Fig. 1A)[19-34]. Theoretically, spin polarization arising from edge dangling bonds has been predicted in pristine zigzag-edged phosphorene nanoribbons (ZPNRs), when non-fully relaxed structure[23]. For in O-terminated case, local edge magnetic moments are predicted to be M_L=0.27 μ_B for the O atom, 0.39 μ_B for the edge P atom, and 0.13 μ_B for its nearest neighbor. O-saturated zigzag PNRs exhibits some edge FM due to the spins of unsaturated bonds in weak P–O bonds along the p_z orbitals in the NR plane, whereas H-terminated zigzag PNRs show no edge FM. This behavior highly contrasts with that of GNMs[12], in which *H*-terminated zigzag edges produce flat-band FM while O-terminated edges exhibiting diamagnetism. Moreover, stronger and more robust edge anti-ferromagnetism (AFM) (0.155 μ_B for the edge P) has been predicted in ZPNRs due to the electronic instability induced by the half-filled 1D bands in absence of Peierls transition[27]. To date none of these theoretical results have been confirmed experimentally.

In this work, flakes of few-layered BPs were mechanically exfoliated from bulk BP (Smart Element Co.) using the Scotch tape method and observed using optical (Fig. 1C) and atomic force microscopes (Fig. 1D) (see Supplementary Material (SM) 3). Following the non-lithographic method used to fabricate GNMs (i.e, using nano-porous alumina template as an etching mask (SM 1-5)[18]), few-layer BPNMs were fabricated (Figs.1B and 1E). Interpore regions correspond to BPNRs, but only two edges of each hexagonal pore can be simultaneously perfect zigzag shaped because of the topological reason that the inner angle of the puckered honeycomb lattice is about ~98.15° (Fig. 1B), and cannot be aligned to the inner angle of the hexagonal pore of 120°. This is different from the case of GNM.

After the formation of nanopore array, the BPNMs were annealed at a critical temperature (T_c) of 300 °C in a high vacuum (~10^{-6} torr) (SM 6) to favor the formation of zigzag pore edges through edge atomic reconstruction. The absence of any substantial background magnetic impurities and magnetic contamination (e.g., Ni, Fe, Co) has been carefully confirmed by the following methods. First, the XPS measurements of three BPNMs reveal no peaks of typical magnetic orbitals (see Fig. 1F). Second, no magnetic hysteresis loops are observed in two different types of few-layer bulk BP flakes (i.e., without pores), namely in type A (main panel of Fig. 2B), produced using the same fabrication processes as for BPNM (Fig. 2A-sample) without pore formation, and type B (inset of Fig. 2B), in which Ar gas etching process was carried out without using a porous alumina template mask as in the case of BPNM). Third, significant differences between magnetization curves for H and O terminated-BPNM are shown in Figs. 2A and 2D, which discard the introduction of magnetic impurities introduced during the fabrication process. Finally, a careful fabrication process strongly reduces the presence of magnetic contamination, since bulk BPs are first mechanically exfoliation and scotch tapes, porous alumina templates use extremely pure Al substrate (99.99 %) for anodic oxidation and its oxidation process, the etching process for pore formation is based Ar gas, and finally only plastic tweezers are used during the fabrication (SM). All of these experimental facts should strongly avoid the presence of parasitic magnetic-background. Subsequently, each BPNM was placed in air atmosphere at 300 K for 2 h, resulting in O-termination of pore edges (i.e., O-termination of the pore edges, because oxidized top layers serve as protection layers of underneath BP layers preventing their bulk oxidation). Immediately following this annealing process, magnetization was measured using superconducting quantum interference devices (Quantum Design Co.).

Figure 2A shows our main measurement findings of the magnetization of the O-terminated BPNM. Ferromagnetic (FMC)-hysteresis loops are clearly observed with $M_s \sim 10^{-4}$ emu/~0.4 cm^2. Such M_s value is approximately 100 times smaller than those in H-terminated FNC GNMs (i.e., $M_s \sim 10^{-6}$ emu)[12,13]. Importantly, the hysteresis loop at T = 2 K approximately remains unchanged even when increasing the temperature up to T = 300 K. On the other hand, few-layer bulk BP flakes without pores do not exhibit any trace of magnetization (main panel and inset of Fig. 2B). These important results indirectly support that the FM observed in Fig. 2A originates solely from the formation of oxidized nano-pores. This has been confirmed at least in three samples.

Since the oxidation of pore edges is easily obtained by exposing BPNM to air atmosphere, one can assume that all pore edges in a BPNM are O-terminated and can become magnetic. If one assumes that the atomic structure of all the pore edge is zigzag and fully O-terminated, then one can estimate a magnetic moment per edge dangling bond in hexagonal pores in order of ~ 1.0 μ_B, where μ_B is the Bohr magneton (SM 9). This value is in good agreement with our ab-initio simulations of the magnetization value of edge P=O bond. Accordingly, BP has a significant advantage in which O-terminate edges generate room-temperature magnetism, in contrast with the much smaller magnetism obtained by partially H-terminated edges in GNM. Figure 2C reveals that the non-annealed BPNM exhibit FMC hysteresis loops with M_s about 4 times lower than those of the T_c-annealed samples (i.e., Fig. 2A). Such result implies that annealing at the T_c is important for introducing large FM. Indeed, reproducibility of magnetism in non-annealed BPNMs is poor with some samples showing M_s values smaller than ~0.3×10^{-4} emu/100 μm^2 (inset of Fig. 2C). In comparison for FMC-GNMs, the zigzag-type edge atomic structure is the most stable structure from both thermal and chemical perspectives[12,16-18], hence annealing at the T_c result in the formation of zigzag pore edges and the subsequent formation of FM after H-termination. The occurrence of similar pore-edge atomic reconstruction to a zigzag geometry is also expected for the pores of our BPNMs (Fig. 1B) following annealing at the T_c, leading to FM after O-termination (Fig. 2A). This is supported by Raman spectroscopy as discussed below.

Figure 2D shows the magnetization curve for the BPNM obtained after annealing under an H_2 atmosphere at 300 °C during 2 h immediately after the formation of nanopores. In contrast to the O-terminated BPNM, the H-terminated BPNM barely exhibit a FMC-hysteresis loop and the magnetic signal is paramagnetic and noisy. Moreover, the M_s of an O-terminated sample subsequently annealed under an H_2 atmosphere at T_c ~ 300 °C for 5 h (Fig. 2E) is ~3 times smaller than that of the original O-terminated sample (Fig.2A). The disappearance of FM in the H-terminated BPNM is consistent with the theoretical prediction of the absence of FM in PNRs with H-terminated zigzag edges. In particular, the result in Fig. 2E suggests that O-termination of the zigzag pore edges is highly stable and cannot be entirely replaced by H-termination.

Temperature-dependence of M_s and magnetization close to residual magnetization (M_r) are shown in Fig. 2F (SM 8). Both M values monotonically increase with decreasing temperature (e.g., from ~0.65×10^{-4} emu/0.4 cm^2 (300K) to ~1.0×10^{-4} emu/0.4 cm^2 (2K) for H = 10 Oe and ~0.7 (300K) to ~1.2 (2K) for H = 200 Oe). Hence, the difference of M_s and M_r between 2K and 300K is evident. This result definitely reinforce the origin of the FMC hysteresis loops observed at 2K and 300K in our O-terminated BPNMs. We finally note that the expected Curie temperatures of measured FMC-BPNMs should be above 350℃, which is the upper limit temperature of our SQUID.

Figure 3 shows the residual magnetization (M_r) of FMC-BPNMs (O-terminated BPNMs) as a function of the interpore distance (*W*), which is identical to the width of a PNR, and M_s as a function of the thickness (*d*) and sample area (*S*). The M_r value appears to be not very sensitive to *W*, despite a very weak decrease with increasing *W* owing to lower pore density (Fig. 3A), which is consistent with previous theories of ZPNRs[23,27] and with our theoretical simulations described below. We note however that this differs from the flat band FM in GNMs, for which the Coulomb exchange interaction between opposite edges strongly decreases with *W*, leading to a loss of the stability of the FMC spin ordering and hence a lower M_r[21]. On the other hand, M_s is seen to increase linearly with *d* and *S* (Figs. 3B and 3C), but the dependence on *d* suggests that M_s becomes negligible in the BPNM mono-layer limit. This could be explained by the strong interlayer interactions in AB stacking of BP (Fig. 1A), favoring the FMC spin configuration, similarly to the case of graphene[25].

Our theoretical calculations for zigzag-PNR actually support this result and also indicate even much stronger interlayer interaction as explained later (Fig. 5E, 5F). This interlayer spin interaction makes long-range spin ordering stable even at 300 K (Fig. 2A). The linear dependence on *S* (Fig. 3C) arises because the area of the O-terminated zigzag pore edges linearly increases with *S*. This means that the fully O-terminated pores uniformly exist through all layers in individual samples. This implies that the O-termination of the pore edges of BPNMs can be easily realized only by exposing samples to air atmosphere and significantly contributes to the observed large-magnitude edge magnetism. Additionally, as discussed above, annealing at T_c may cause the reconstruction of the pore-edge atomic structure, resulting in formation of zigzag pore edges and subsequent formation of FM after O-termination. Because the BPNM tends to disappear when annealing at T > 350 °C, the annealing temperature of 300 °C is approximately the temperature T_c at which the reconstruction of pore-edge atomic structures takes place in BPNMs. In comparison, T_c is much lower than ~800 °C for the FMC-GNMs.

The analysis of typical Raman spectra of BPNMs, exhibiting or not a FM signal, give further support to the above argument (Fig. 4A). From Fig. 4A, it is confirmed that the heights of the band peaks due to the phonons resulting from interlayer interactions (I_{Ag1}) are nearly the same in the spectra of the two samples, while the intensity of the band attributed to the phonon from the Si substrate (I_{Si}) is significantly larger in the non-FMC sample, leading to a low I_{Ag1}/I_{Si} value. We find that this tendency agrees with that from the bulk regions and edges of few-layer BP flakes (i.e., without nano-pores) of different *d* not annealed at T_c (Fig. 4B). Fig. 4B implies that the I_{Ag1}/I_{Si} ratios observed at the edges are lower than those of the corresponding bulk regions in nearly all of the samples (Inset), and an approximately linear correlation between the I_{Ag1}/I_{Si} ratio and *d* is obtained[22]. The lower I_{Ag1}/I_{Si} values at the edges can be obtained from the same relationship as that in Fig. 4A (i.e., the higher peak value of I_{Si}). Indeed, the I_{Ag1}/I_{Si} values for the FMC (○) and non-FMC (×) BPNMs, including those shown in Fig. 4A, follow the peak trends for the bulk regions and edges plotted in Fig. 4B, respectively.

The lower I_{Ag1}/I_{Si} values at the edges of BP flakes can be attributed to the following two possibilities; namely the presence of the armchair-rich edges or the influence of the scattered laser beam from the Si substrate. The first possibility originates from the following two reasons. First, since the BP flakes without nano-pores were just mechanically exfoliated from bulk BP without any intentional alignment of crystal axis and not by annealing at the T_c, the edge atomic structures should be rough edges but preferentially of armchair type. This is because zigzag edge appears only when crystal axis is perfectly

aligned along Y axis in Fig. 1A, while in any other cases the buckling armchair edge appears. Second, the intensity of the phonons from the Si substrate at armchair edges is higher than that of phonons at the zigzag edges, because the buckling armchair structures are formed along z-axis (Fig. 1A) and the surface of the Si substrate can easily oscillate under them (e.g., beneath gray P atoms). Indeed, the phonon dispersion along the zigzag direction was shown to be sharper than that along the armchair direction using first-principles calculations for BP[26]. However, these effects are suppressed in the bulk region in few layer BPs and, hence, the I_{Ag1}/I_{Si} values are not high. On the other hand, all phonons are more effectively activated at sample edges than in the bulk regions. This effect should be more significant for phonon arising from Si substrate under the buckling armchair structure for the abovementioned reasons. On the other hand, the second possibility directly results in high I_{Si} signals. As mentioned above, the I_{Ag1}/I_{Si} values for the FMC and non-FMC BPNMs follow the peak trends for the bulk regions and edges plotted in Fig. 4B. Because the pore structures (i.e., diameter and hexagonal shape) observed by SEM and AFM are almost the same in these two-type BPNMs, the contribution of such second possibility should be also the same. This cannot explain different I_{Si} in Fig. 4. Therefore, possibility (1) is the origin for Fig. 4.

Hence, the low I_{Ag1}/I_{Si} ratios arising from the high I_{Si} values in Fig. 4A suggest the buckling armchair-rich pore edges in the non-FMC BPNM. In contrast, it can be concluded that the pore edge of the FMC BPNMs is zigzag rich, resulting from edge reconstruction during annealing at T_c. This also suggests the formation of partial zigzag edges in other pore edges in addition to the two zigzag pore edges (inset of Fig. 2A) (SM 7). Only two out of ten BPNMs did not result in zigzag-rich pore edges after annealing at T_c (SM 7). This also suggests that the buckling armchair edge requires higher energy for stability after the T_c annealing and therefore is hard to be realized. The reconstruction by the T_c annealing may introduce relaxed structure to interpore BPNRs, which conventionally results in Peierls transition and disappearance of magnetism[24, 27]. However, the present BPNM structure, in which six BPNRs with a typical width ~20nm form one hexagonal unit cell leaving a nanopore at the center, may prevent occurrence of Peierls transition.

We now theoretically investigate the presence of edge-magnetism in O-terminated ZPNRs by performing first principles calculations (SM 10). Figure 5A shows the band structure of the relaxed O-terminated 10-ZPNRs (Fig. 5B) considered in our calculations. The left and right panels correspond to the spin-unpolarized and -polarized cases, respectively. Similarly to previous calculations, a pair of midgap states (red arrow in Fig.5A) span across the band gap and cross the Fermi level at around $\pi/2a$ of the Brillouin zone (BZ) inducing a metallic state. The midgap states at Γ and X (right panel of Fig. 5A) are completely localized along the edges as seen in Figs.5B and 5C. This is related to the small band splitting observed at the Γ-point for O-terminated PNRs, which is much smaller than [24], and implies a strong reduction of inter-edge coupling in presence of O. This is in agreement with Fig.3A.

We have also checked inter-edge magnetic coupling for both parallel and antiparallel couplings of edge-FMC and edge-Anti-FMC (AFMC) configurations in the doubly relaxed unit cells. We found that the total energies were very similar ($\Delta E < 1$ meV), which highlights the small spin interaction between edges. The edge-FMC configuration with antiparallel inter-edge coupling (similar to zigzag GNRs) always led to non-magnetic or bad converged solutions. In contrast, the edge-AFMC configuration always converged very fast while keeping the initial AFMC guess along the edge. Interestingly, the O atoms were not initially polarized and became magnetic during the self-consistency calculation. The magnetic moments emerging at the O atoms couple ferromagnetically with the ones at the neighboring P_{edge} atoms giving rise to a huge enhancement of the edge magnetism (the green arrows in Fig. 5C; SM 10). The values of the local magnetic moment M_L at the P_{edge} and O atoms for the O-terminated 10-ZPNR are $|M_P| = 0.55\ \mu_B$ and $|M_O| = 0.4\ \mu_B$, respectively (very similar to the O-terminated 6-ZPNR). The calculated total M_L is around 1 μ_B per P=O dimer, almost seven times bigger than those in Ref [27]. We also reveal that at the X-point the spin densities from the valence bands are only localized along the edges of the NR which strongly contributes to the edge-Anti-FMC state (SM 10). Although the M_L value is only a few times larger than that of the FMC-GNMs ($M_L \sim 0.2$ or $0.3\ \mu_B$)[12], the uniform oxidation of pore edges through all layers in a BPNM allows this large magnetism. Since the H-termination eliminates the abovementioned unsaturated bond, magnetism disappears.

Interlayer edge-spin coupling in the O-terminated ZPNRs also strongly contributes to the FM as shown in Figs. 5C and 5D (SM 10). Misalignment of interlayer adjacent O=P_{edge} atoms in AB stacking allows FMC spin configuration in bilayer ZPNRs (Fig. 5C) as well as the case of few-layer GNRs. However, the strong interlayer interaction due to the O atom (SM 9) induces this FMC spin alignment and makes spin ordering more stable. Indeed, the linear scaling of the absolute

magnetization, defined as the sum of the absolute values of the M_L (m_i) on each atom, $|M| = \Sigma_i |m_i|$, is confirmed with the number of layers (N) as shown in Fig.5D. This is qualitatively consistent with Fig. 3B.

In conclusion, our results suggest the formation of room-temperature edge ferromagnetism in O-terminated BPNMs that is ~100 times/area larger than that reported for FM-GNMs. In contrast to H-terminated GNMs where edge hydrogenation is delicate under H_2 atmosphere and not very stable, O-termination of BPNMs is robust in air atmosphere. Moreover, while O-termination suppresses magnetization in GNMs, oxidation enhances edge magnetism in BPNMs. Therefore, the emergence of magnetization with O-termination should be significantly advantageous compared to the H-termination in GNMs for the generation of edge magnetism in low-dimensional materials. Experimental results are supported by first principles calculations which suggest that that the ferromagnetic coupling of edge P atom with O atom and the strong spin localization of edge valence band could be at the origin of colossal edge magnetism. Besides, interlayer interaction induces FM spin alignment and makes spin ordering stable. Finally our results (an increasing of magnetism with increasing pore density) are consistent with an oxidation process of our samples limited to the top surface and pore edges, leaving the deepest layers intact. Such limitation of black phosphorus oxidization on the surface has been already discussed in the literature[31].

Edge magnetism in molybdenum disulfide (MoS_2) was also reported[35]. However, it was much different from the present case. For example, ferromagnetic hysteresis loop of the result was not evident in the work. Moreover, the M-H curves provided a component of the large diamagnetism background signal. Consequently, these results differ substantially from having a large hysteresis loop with less diamagnetic background, as in our study. Furthermore, in our work the formation of the FM state can be tuned by a different type of chemical treatment (using O- or H-termination), acting preferentially on the pores edges. This is difficult in MoS_2. The formation and the control of a room temperature magnetic order in 2D materials stand as genuine milestones, and our reported realization of room-temperature ferromagnetism (without using rare-earth magnetic atoms) in oxidized-BPNMs is therefore highly valuable for the development of future innovative magnetic- and spintronic-based technologies.

Author information

Corresponding author: E-mail J-haru@ee.aoyama.ac.jp

Author contributions

Y. N., C. O., R. I., Y. K., K. N., and T. N. performed experiments. D. S. performed the theoretical calculations. J. H., S. K., S. R. designed the experiments, analyzed the data, and wrote the manuscript

Notes

The authors declare no competing financial interest.

Acknowledgements

The authors thank J. Akimitsu, K. Horigane, T. Muranaka, Y. K. Fukai, T. Enoki, M. Yamamoto, S. Tarucha, T. Ando, A. H. Macdonald, P. Seneor, R. Wiesendanger, and M. S. Dresselhaus for their technical contributions, fruitful discussions, and encouragements. This work at Aoyama Gakuin was partly supported by a Grant-in-aid for Scientific Research (Basic research A: 24241046) and grant for private University in MEXT and AOARD grant (135049) in U.S. Air Force Office of Scientific Research. The Tokyo University's work was also supported by the Special Coordination Funds for Promoting Science and Technology. S.R. acknowledge the Spanish Ministry of Economy and Competitiveness for funding (MAT2012-33911), the Secretaria de Universidades e Investigación del Departamento de Economia y Conocimiento de la Generalitat de Catalunya and the Severo Ochoa Program (MINECO SEV-2013-0295), and funding from the European Union Seventh Framework Programme under Grant agreement No. 604391 Graphene Flagship.

References

1. Ferrari, A. C. *et al.*, *Nanoscale*, **7**, 4587 (2015).
2. Roche S *et al.*, *2D Materials* 2, 030202 (2015)

3. Yang H. X. *et al., Phys. Rev. Lett. 110, 046603 (2013).*
4. Avsar, A. *et al., Nature Comm. 5, 4875 (2014).*
5. Lin, C. *et al., Nano Lett. **15**, 903 (2015).*
6. Zsolt, G. et al., *Nature 514, 608 (2014)*
7. Nakada, K., Fujita, M., Dresselhaus, G., and Dresselhaus, M. S., *Phys. Rev. B.* 1996, **54,** 17954.
8. Soriano, D. *et al., Phys. Rev. Lett.* 2011, **107**, 016602.
9. Lee, H. *et al., Chem. Phys. Lett.* 2004, **398**, 207.
10. Kusakabe, K. and Maruyama, M., *Phys. Rev. B.* 2003, **67**, 092406.
11. Shimizu, T., Haruyama, J. *et al., Nature Nanotech*. 2011, **6,** 45.
12. Tada, K., Haruyama, J., Chshiev, M. *et al, Phys. Status Solidi B.* 2012, **249**, 2491.
13. Kato, T., Nakamura, T., Haruyama, J. *et al., Appl. Phys. Lett*. 2014, **104**, 252410.
14. Hashimoto, T., Haruyama, J., Soriano, D., Roche, S. *et al., Appl. Phys. Lett*. 2014, **105**, 183111.
15. Hashimoto, T., Haruyama, J. *et al., Mat. Sciences and Appl.* 2014, **5(1)**, 1.
16. Jia, X., Dresselhaus, M. S. *et al., Science.* 2009, **323**, 1701.
17. Girit , C. O. *et al., Science.* 2009, **323**, 1705.
18. You, Y., Ni, Z., Yu, T. and Shen, Z. *Appl. Phys. Lett.* 2008, **93,** 163112.
19. Li, L. *et al., Nature Nanotech*. 2014, **9**, 372.
20. Herrero, P.-J. *et al., Nature Nanotech*. 2014, **9**, 330.
21. Koenig, S. P. *et al., Appl. Phys. Lett*. 2014, **104**, 103106.
22. Gomez, A. C. *et al., 2D Materials* 2014, **1**, 025001 .
23. Zhu, Z. *et al., Appl. Phys. Lett*. 2014, **105**, 113105.
24. Peng, X. *et al., J. Appl. Phys*. 2014, **116**, 144301.
25. Carvalho, A., Rodin, A. S., and Neto, A. H. C., *Euro. Phys. Lett.* 2014, **108**, 47005.
26. Ong, Z. Y., Cai, Y., Zhang, G., Zhang, Y. –W., arXiv:1409.097..
27. Du, Y. *et al., Sci. Rep.* 2015, **5**, 8921.
28. Zhu, W. *et al., Nano Lett.* 2015, **15**, 1883.
29. Dai, J. and Zeng, X. C., *J. Phys. Chem. Lett.* 2014, **5**, 1289.
30. Luo, X., Lu, X., *et al., Nano Letters.* 2015, **15**, 3931.
31. Ziletti, A., Castro Neto, A. H. *et al., Phys. Rev. B*. 2015, **91**, 085407.
32. Liu, H. *et al, ACS Nano* 2014, **8** (4), 4033.
33. Gillgren, N. *et al., 2D Mater.* 2015, **2** (1), 011001.
34. Zhu, Z. and Tomanek, D., *Phys. Rev. Lett.* 2014, **112** (17), 176802.
35. Tongay, S., *et al., Appl. Phys. Lett*. 2012, **101**, 123105.

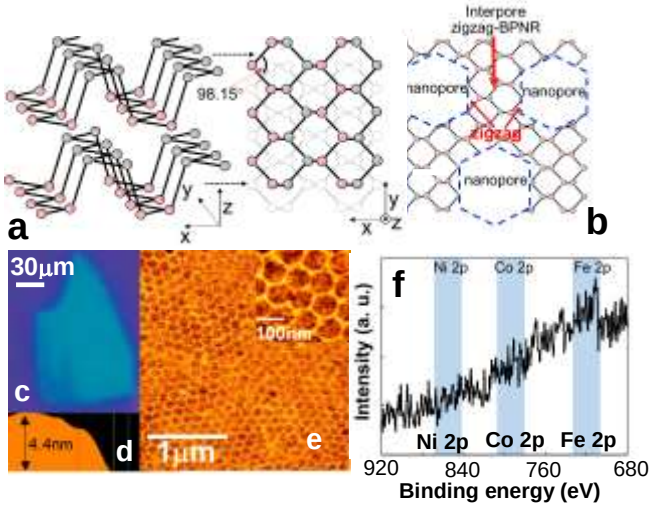
Interpore
zigzag-BPNR
nanopore
nanopore
zigzag
nanopore
98.15°
a
b
30μm
c
4.4nm
d
1μm
100nm
e
f
Ni 2p
Co 2p
Fe 2p
Intensity (a. u.)
Ni 2p
Co 2p
Fe 2p
920
840
760
680
Binding energy (eV)

Fig. 1

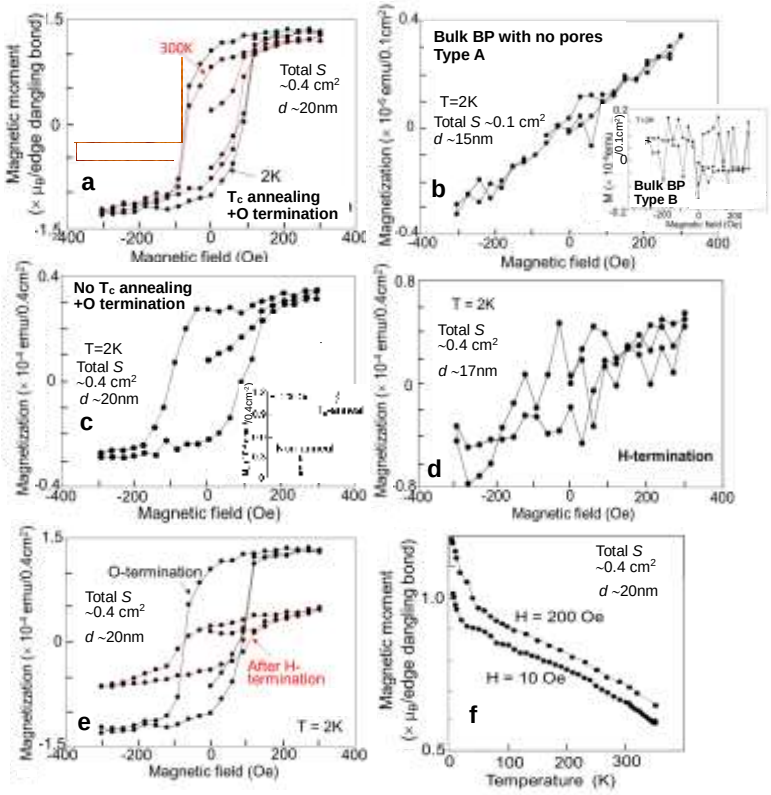
Magnetic moment (× μB/edge dangling bond)
300K
Total S ~0.4 cm²
d ~20nm
2K
Tc annealing
+O termination
a
Magnetic field (Oe)
Bulk BP with no pores
Type A
T=2K
Total S ~0.1 cm²
d ~15nm
b
Bulk BP
Type B
Magnetization (× 10⁻⁶ emu/0.1cm²)
No Tc annealing
+O termination
T=2K
Total S ~0.4 cm²
d ~20nm
c
Magnetization (× 10⁻⁴ emu/0.4cm²)
T = 2K
Total S ~0.4 cm²
d ~17nm
H-termination
d
O-termination
Total S ~0.4 cm²
d ~20nm
After H-termination
T = 2K
e
Total S ~0.4 cm²
d ~20nm
H = 200 Oe
H = 10 Oe
f
Temperature (K)

Fig. 2

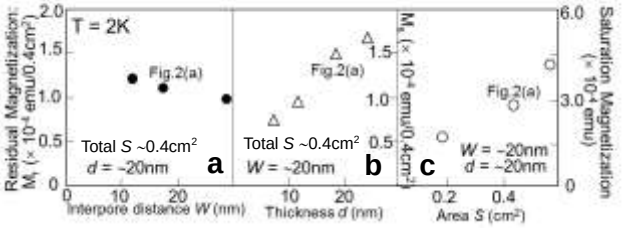
T = 2K
Fig.2(a)
Total S ~0.4cm²
d = ~20nm
a
Interpore distance W (nm)
Residual Magnetization: Mr (× 10⁻⁴ emu/0.4cm²)
Fig.2(a)
Total S ~0.4cm²
W = ~20nm
b
Thickness d (nm)
Fig.2(a)
W = ~20nm
d = ~20nm
c
Area S (cm²)
Saturation Magnetization (× 10⁻⁴ emu)

Fig. 3

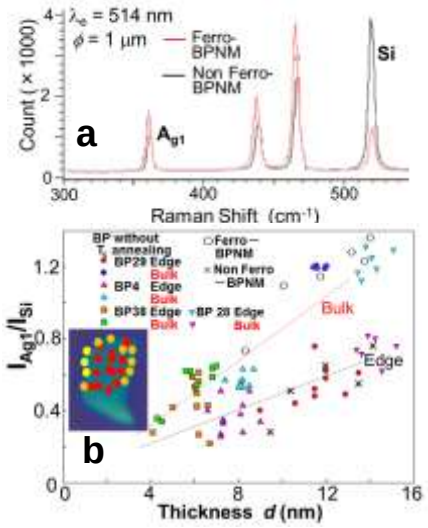
λe = 514 nm
ϕ = 1 μm
Ferro-BPNM
Non Ferro-BPNM
Si
a
Ag1
Count (× 1000)
Raman Shift (cm⁻¹)
BP without T annealing
BP29 Edge
Bulk
BP4 Edge
Bulk
BP38 Edge
Bulk
Ferro-BPNM
Non Ferro-BPNM
BP 28 Edge
Bulk
Bulk
Edge
b
IAg1/ISi
Thickness d (nm)

Fig. 4

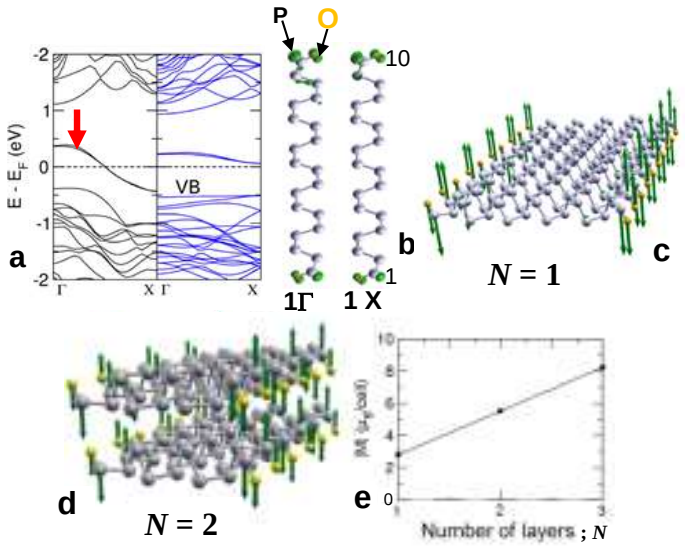

Fig. 5

Figure captions

Fig. 1 **(a)** Schematic cross-sectional and top views of a puckered honeycomb lattice of two-layer black phosphorens with AB stacking. Gray and red symbol's P atoms locate within different height. Zigzag edge is within mono layer along y axis, while buckling arm chair edge is formed to z-axis direction along x axis. **(b)** Schematic top view of a BPNM, in which two pore edges are perfectly aligned to zigzag structure. In actual structure, pore size and interpore spacing are much larger and larger number of P atoms exists at the interpore BPNR regions. **(c)** Example of optical microscope image of a flake of few-layer BP mechanically exfoliated from bulk BP. **(d)** Cross-sectional image of (c) obtained using atomic-force microscope. One sample consists of main large flakes and other many small flakes with number of $10\sim10^2$ (SM 3). Thickness and area of all flakes including small flakes have been measured so as to be 0.1 ~0.4 cm^2 of the total area with similar thickness in one sample. **(e)** Atomic-force microscope top-view image of a BPNM with a large number ($\sim10^{12}$) of pores, which was fabricated via. non-lithographic method (SM1-5) in an extremely careful way (e.g., using plastic tweezers) to avoid incorporating magnetic impurities, defects, and contamination. **Inset:** Higher magnification image. **(f)** XPS spectra of a ferromagnetic BPNM. The binding energies have been calibrated at the Si 2p level in SiO_2 (103.3 eV). $2p_{3/2}$-binding Energies are 853.8 eV for Ni in NiO_2, 780.4 eV for Co in CoO, and 710.9 eV Fe in Fe_2O_3.

Fig. 2 **(a, c-e),** Magnetization curves for BPNMs with **(a)** T_c annealing and O-termination, **(c)** no T_c annealing and O-termination, **(d)** H-termination, **(e)** H-termination of the sample in (a). Y-axis of Figs. 2a and 2f has been normalized by number of O-terminated edge dangling bond of pores (SM 9). **Inset of (c),** Saturation magnetization (M_s) of T_c- and no T_c-annealed BPNMs (each five samples) BPNMs at 2K. **(b)** Magnetization curve for Type-A few-layer bulk BP flake obtained through all the same fabrication process as those for (a)-sample except for the pore formation. **Inset of (b)**; Magnetization for Type-B bulk thick BP, in which Ar gas etching process was carried out without using porous alumina template mask by the same Ar gas condition as that for pore forming. For all samples, no background magnetism was subtracted except for (c), in which a diamagnetic background line was subtracted. *S* is the sample area including the total pore area. Results of Fig. 2(b) are independent of *S*. **(f)** Temperature dependence of magnetization values of a magnetic BPNM (i.e., with T_c annealing and O-termination) measured with decreasing temperatures.

Fig. 3 **(a)** Residual magnetization (M_r) of FM BPNMs as a function of the interpore distance (*W*) (i.e., width of the interpore PNR regions), and M_s as a function of the **(b)** thickness (*d*) and **(c)** sample area (*S*). Fig.2(a)-sample is noted on individual figures. *W* has been controlled by that in porous alumina template mask formed by changing temperature of anodic oxidation of Al substrate e.g., (0 ~ 10℃). In contrast, samples with different *d* and *S* have been selected from many random samples.

Fig. 4 **(a)** Typical micro Raman spectra for two BPNMs that do and do not exhibit FM. **(b)** Correlation of the *d* and I_{Ag1}/I_{Si} values in the Raman spectra measured in the bulk and at the edges of three few-layer BP flakes (i.e., without nanopores) without T_c annealing. The linear dotted lines indicate trends for the individual correlations. The I_{Ag1}/I_{Si} values for the FM (○) and non FM (×) BPNMs, including the result of Fig. 4(a), are also noted. **Inset:** Example of Raman mapping for sample BP4 in main panel. Red, orange, and yellow symbols mean the measured points with results of $I_{Ag1}/I_{Si} > 0.5$, $0.5 > I_{Ag1}/I_{Si} > 0.3$, $0.3 > I_{Ag1}/I_{Si}$, respectively.

Fig. 5 **(a)** Band structures for O-terminated 10-ZPNR. Left and right panels correspond to spin-unpolarized and -polarized cases (SM10). **(b)** Charge density contribution (shown in green) of one of the midgap states (red arrow in (a)) at Γ and X. The structure corresponds to O-terminated interpore ZPNR region of BPNM. Distances are very similar to those reported for mono-layer PNR. The distance between P and O atoms at the edges is 1.5 Å, which corresponds to a P=0 double bond. **(c, d)** Illustration of the edge anti-FM emerging at **(c)** the mono-layer zigzag edges corresponding to (b) and **(d)** the bi-layers. Green arrows correspond to the spin magnetic moment computed on each atom. **(e)** Scaling of the absolute magnetization per unit cell with number of layers (*N*). Relaxed interlayer-distance ($d_z \approx 0.198$ nm) is around 0.1 nm shorter than previously report.